

# On the Diversity of OTFS Modulation in Doubly-Dispersive Channels

G. D. Surabhi, Rose Mary Augustine, and A. Chockalingam  
Department of ECE, Indian Institute of Science, Bangalore 560012

**Abstract**—Orthogonal time frequency space (OTFS) is a 2-dimensional (2D) modulation technique designed in the delay-Doppler domain. A key premise behind OTFS is the transformation of a time varying multipath channel into an almost non-fading 2D channel in delay-Doppler domain such that all symbols in a transmission frame experience the same channel gain. It has been suggested in the recent literature that OTFS can extract full diversity in the delay-Doppler domain, where full diversity refers to the number of multipath components separable in either the delay or Doppler dimension, but without a formal analysis. In this paper, we present a formal analysis of the diversity achieved by OTFS modulation along with supporting simulations. Specifically, we prove that the asymptotic diversity order of OTFS (as  $\text{SNR} \rightarrow \infty$ ) is one. However, in the finite SNR regime, potential for a higher order diversity is witnessed before the diversity one regime takes over. Also, the diversity one regime starts at lower BER values for increased frame sizes. We also propose a phase rotation scheme for OTFS using transcendental numbers. We show that OTFS with this proposed scheme extracts the full diversity in the delay-Doppler domain.

**Keywords** – OTFS modulation, 2D modulation, delay-Doppler domain, diversity order, phase rotation, MIMO-OTFS.

## I. INTRODUCTION

Future wireless communication systems are envisioned to support diverse requirements that include high mobility application scenarios such as high-speed train, vehicle-to-vehicle, and vehicle-to-infrastructure communications. The dynamic nature of wireless channels in such scenarios makes them doubly-dispersive, with multipath propagation effects causing time dispersion and Doppler shifts causing frequency dispersion [1]. Conventional multicarrier modulation techniques such as orthogonal frequency division multiplexing (OFDM) mitigate the effect of inter-symbol interference (ISI) caused due to time dispersion. However, the performance of OFDM systems depends significantly on the orthogonality among the subcarriers. Doppler shifts can destroy the orthogonality among the subcarriers, resulting in inter-carrier interference (ICI) which degrades performance [2].

Orthogonal time frequency space (OTFS) modulation is a recently proposed modulation scheme [3]-[7] that uses delay-Doppler domain for multiplexing the information symbols instead of time-frequency domain as in conventional modulation schemes. OTFS modulation uses transformations that spread information across the delay-Doppler plane. This spreading across the delay-Doppler plane converts a doubly-dispersive channel into an almost non-fading channel in the delay-Doppler domain. The relatively constant channel gain experienced by all the symbols in an OTFS transmission frame

can greatly reduce the overhead on the channel estimation in a rapidly time varying channel. Another attractive feature of OTFS from an implementation viewpoint is that OTFS modulation can be architected over any multicarrier modulation (e.g., OFDM) by using additional pre-processing and post-processing blocks [5].

OTFS has been shown to achieve significantly better error performance compared to OFDM for vehicle speeds ranging from 30 kmph to 500 kmph in 4 GHz band [3]. It has also shown to perform well in mmWave frequency bands [7]. Owing to the simplicity of implementation and robustness to Doppler spreads, several works on OTFS have started emerging in the recent literature [8]-[12]. OTFS systems using OFDM as the inner core have been considered in [8],[9]. In [10],[11], the robustness of OTFS modulation has been demonstrated in high Doppler fading channels, using low complexity signal detection techniques. While [10] proposed a message passing based algorithm for OTFS signal detection, [11] proposed a Markov Chain Monte Carlo based algorithm for detection and a pseudo-random noise (PN) pilot based scheme for channel estimation in the delay-Doppler domain. The above detection algorithms were devised using a system model based on the vectorized input-output relation for OTFS [10]. Signal detection and channel estimation for multiple-input multiple-output OTFS (MIMO-OTFS) have been considered in [12], where it has been shown MIMO-OTFS offers significantly better performance compared to MIMO-OFDM.

While recent papers on OTFS have demonstrated the performance superiority of OTFS over OFDM, a formal analysis and claim on the diversity order achieved by OTFS is yet to appear. It has been suggested in [4] that OTFS can achieve full diversity in the delay-Doppler domain, where full diversity refers to the number of clustered reflectors in the channel (in other words, the number of multipath components separable in either the delay or Doppler dimension). However, this suggestion has not been established through analysis or simulation. Filling this gap, our contribution in this paper provides a formal analysis of the diversity order achieved by OTFS in doubly-dispersive channels with supporting simulation results. The key findings and contributions in this work can be summarized as follows.

- We first derive the diversity order of OTFS in a single-input single-output (SISO) setting with maximum likelihood (ML) detection. It is shown that the asymptotic diversity order of OTFS (as  $\text{SNR} \rightarrow \infty$ ) is one. Though the asymptotic diversity order is one, potential for a

higher order diversity is witnessed in the finite SNR regime before the diversity one regime takes over. Also, it is observed that the diversity one regime starts at lower BER values for increased frame sizes. A lower bound on the BER computed by summing up the pairwise error probabilities corresponding to all pairs of data matrices whose difference matrices have rank one provides an analytical support for this observation.

- Next, in an attempt to extract full diversity in the asymptotic regime, we propose a phase rotation scheme for OTFS using transcendental numbers. It is shown that OTFS with this proposed scheme extracts the full diversity in the delay-Doppler domain.
- Finally, we extend the diversity analysis to MIMO-OTFS and show that the asymptotic diversity order of MIMO-OTFS is equal to the number of receive antennas. We also extend the phase rotation scheme to MIMO-OTFS system to extract full diversity in the delay-Doppler domain.

The rest of the paper is organized as follows. The OTFS modulation scheme is presented in Sec. II. The diversity analysis of OTFS in SISO setting and corresponding simulation results are presented in Sec. III. The proposed phase rotation scheme that achieves full diversity is presented in Sec. IV. The MIMO-OTFS system, its asymptotic diversity order, and phase rotation scheme are presented in Sec. V. Conclusions are presented in Sec. VI.

## II. OTFS MODULATION

The fundamental feature of OTFS modulation that distinguishes it from other time-frequency (TF) modulation schemes is the use of delay-Doppler domain for multiplexing the modulation symbols. The channel representation is also in the delay-Doppler domain. The complex baseband channel impulse response in delay-Doppler domain is denoted by  $h(\tau, \nu)$ , where  $\tau$  and  $\nu$  are the delay and Doppler variables, respectively. With this representation, the received signal  $y(t)$  due to a transmit signal  $x(t)$  is given by

$$y(t) = \int_{\nu} \int_{\tau} h(\tau, \nu) x(t - \tau) e^{j2\pi\nu(t - \tau)} d\tau d\nu. \quad (1)$$

The block diagram for OTFS modulation scheme is shown in Fig. 1. The inner box in the block diagram is the familiar multicarrier TF modulation and the outer box with pre- and post-processor is the OTFS modulator that operates in the delay-Doppler domain. At the transmitter, the information symbols (e.g., QAM symbols) denoted by  $x[k, l]$  residing in delay-Doppler domain are mapped to the TF signal  $X[n, m]$  through the 2D inverse symplectic Fourier transform (ISFFT) and windowing. Subsequently, this TF signal is transformed into a time domain signal  $x(t)$  through Heisenberg transform for transmission. At the receiver, the received signal  $y(t)$  is transformed back to a TF domain signal  $Y[n, m]$  through Wigner transform (inverse Heisenberg transform). The TF signal  $Y[n, m]$  thus obtained is mapped to the delay-Doppler domain signal  $y[k, l]$  using the symplectic finite Fourier transform (SFFT) for demodulation. In the subsequent subsections,

we describe the TF modulation and the OTFS modulation in detail.

### A. Time-frequency modulation

- The time-frequency plane is sampled at intervals  $T$  and  $\Delta f$ , respectively, to obtain a 2D lattice or grid  $\Lambda$ , which can be defined as

$$\Lambda = \{(nT, m\Delta f), n = 0, \dots, N-1, m = 0, \dots, M-1\}. \quad (2)$$

- The signal in TF domain  $X[n, m]$ ,  $n = 0, \dots, N-1$ ,  $m = 0, \dots, M-1$  is transmitted in a given packet burst, which has duration  $NT$  and occupies a bandwidth of  $M\Delta f$ .
- Let  $g_{tx}(t)$  and  $g_{rx}(t)$  denote the transmit and receive pulses, respectively. We assume  $g_{tx}(t)$ ,  $g_{rx}(t)$  to be bi-orthogonal with respect to translations by integer multiples of time  $T$  and frequency  $\Delta f$ , i.e.,

$$\int e^{-j2\pi m\Delta f(t-nT)} g_{rx}^*(t-nT) g_{tx}(t) dt = \delta(m)\delta(n). \quad (3)$$

The bi-orthogonality property of the pulse shapes ensures that the cross-symbol interference is eliminated in the symbol reception.

- TF modulation: The signal in TF domain  $X[n, m]$  is transformed to the time domain signal  $x(t)$  through the Heisenberg transform given by

$$x(t) = \sum_{n=0}^{N-1} \sum_{m=0}^{M-1} X[n, m] g_{tx}(t-nT) e^{j2\pi m\Delta f(t-nT)}. \quad (4)$$

- TF demodulation: At the receiver, the sufficient statistic for symbol detection is obtained by matched filtering the received signal with the receive pulse  $g_{rx}(t)$ . This requires the computation of the cross-ambiguity function  $A_{g_{rx}, y}(\tau, \nu)$ , given by

$$A_{g_{rx}, y}(\tau, \nu) = \int g_{rx}^*(t - \tau) y(t) e^{-j2\pi\nu(t - \tau)} dt. \quad (5)$$

Sampling this function on the lattice  $\Lambda$  yields the matched filter output, given by

$$Y[n, m] = A_{g_{rx}, y}(\tau, \nu)|_{\tau=nT, \nu=m\Delta f}. \quad (6)$$

Equation (6) is called the Wigner transform, which can be looked at as the inverse of the Heisenberg transform.

- If  $h(\tau, \nu)$  has finite support bounded by  $(\tau_{\max}, \nu_{\max})$  and if  $A_{g_{rx}, g_{tx}}(\tau, \nu) = 0$  for  $\tau \in (nT - \tau_{\max}, nT + \tau_{\max})$ ,  $\nu \in (m\Delta f - \nu_{\max}, m\Delta f + \nu_{\max})$ , the relation between  $Y[n, m]$  and  $X[n, m]$  for TF modulation can be derived as [4]

$$Y[n, m] = H[n, m]X[n, m] + V[n, m], \quad (7)$$

where  $V[n, m]$  is the additive white Gaussian noise at the output of the matched filter and  $H[n, m]$  is given by

$$H[n, m] = \int_{\tau} \int_{\nu} h(\tau, \nu) e^{j2\pi\nu nT} e^{-j2\pi(\nu + m\Delta f)\tau} d\nu d\tau. \quad (8)$$

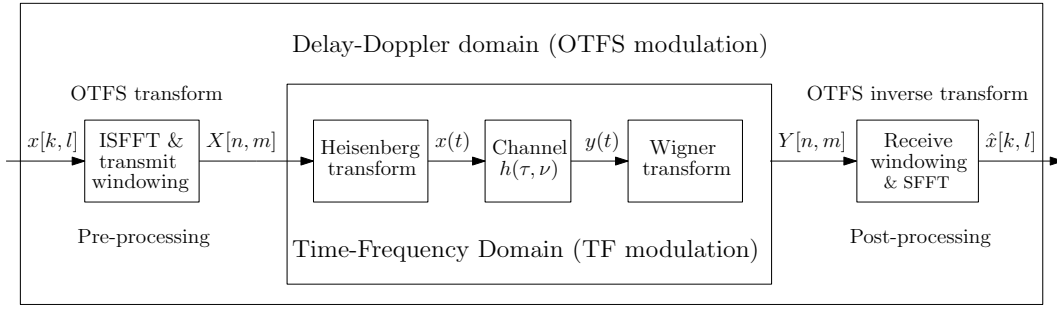


Fig. 1: OTFS modulation scheme.

From (7), note that  $X[n, m]$  is not affected by cross-symbol interference either in time or in frequency. In the absence of noise, the received symbol  $X[n, m]$  is same as the transmitted symbol except for the complex scale factor  $H[n, m]$ . Note that the complex scale factor  $H[n, m]$  is a weighted superposition of Fourier exponential functions. This relation can be formally expressed via a two dimensional transform called the symplectic Fourier transform.

### B. OTFS modulation

In this subsection, we describe the OTFS modulation and demodulation.

- Let  $X_p[n, m]$  denote the periodized version of  $X[n, m]$  with period  $(N, M)$ . The SFFT of  $X_p[n, m]$  is defined as

$$x_p[k, l] = \sum_{n=0}^{N-1} \sum_{m=0}^{M-1} X_p[n, m] e^{-j2\pi(\frac{nk}{N} - \frac{ml}{M})}, \quad (9)$$

and ISFFT of  $X_p[n, m] = SFFT^{-1}(x[k, l])$  is defined as

$$X_p[n, m] = \frac{1}{MN} \sum_{k=0}^{N-1} \sum_{l=0}^{M-1} x[k, l] e^{j2\pi(\frac{nk}{N} - \frac{ml}{M})}. \quad (10)$$

- OTFS transform: The information symbols in the delay-Doppler domain  $x[k, l]$  are mapped to TF domain symbols  $X[n, m]$  as follows:

$$X[n, m] = W_{tx}[n, m] SFFT^{-1}(x[k, l]), \quad (11)$$

where  $W_{tx}[n, m]$  is the transmit windowing square summable function.

- $X[n, m]$  thus obtained is in TF domain and is TF modulated as described in the previous subsection for transmission through the channel.
- OTFS demodulation: The received signal  $y(t)$  is transformed into  $Y[n, m]$  using Wigner filter as described by (6). A receive window  $W_{rx}[n, m]$  is applied to  $Y[n, m]$  to obtain  $Y_W[n, m] = W_{rx}[n, m] Y[n, m]$ . This is periodized to obtain  $Y_p[n, m]$  with period  $(N, M)$ , given by

$$Y_p[n, m] = \sum_{k, l=-\infty}^{\infty} Y_W[n - kN, m - lM]. \quad (12)$$

- The symplectic finite Fourier transform is then applied to  $Y_p[n, m]$  to convert it from TF domain back to delay-Doppler domain to obtain  $\hat{x}[k, l]$  as

$$\hat{x}[k, l] = SFFT(Y_p[n, m]). \quad (13)$$

Using the equations (4)-(13), the input-output relation in OTFS modulation can be derived as [3]

$$\hat{x}[k, l] = \frac{1}{MN} \sum_{m=0}^{M-1} \sum_{n=0}^{N-1} x[n, m] h_w \left( \frac{k-n}{NT}, \frac{l-m}{M\Delta f} \right) + v[k, l], \quad (14)$$

where

$$h_w \left( \frac{k-n}{NT}, \frac{l-m}{M\Delta f} \right) = h_w(\nu', \tau') \Big|_{\nu' = \frac{k-n}{NT}, \tau' = \frac{l-m}{M\Delta f}}, \quad (15)$$

where  $h_w(\nu', \tau')$  is the circular convolution of the channel response with a windowing function  $w(\tau, \nu)$ , given by

$$h_w(\nu', \tau') = \int_{\nu} \int_{\tau} h(\tau, \nu) w(\nu' - \nu, \tau' - \tau) d\tau d\nu, \quad (16)$$

and  $w(\tau, \nu)$  is given by

$$w(\tau, \nu) = \sum_{m=0}^{M-1} \sum_{n=0}^{N-1} W_{tx}[n, m] W_{rx}[n, m] e^{-j2\pi(\nu nT - \tau m\Delta f)}. \quad (17)$$

### C. Vectorized formulation of the input-output relation

Consider a channel with  $P$  paths, resulting from  $P$  clusters of reflectors, where each reflector is associated with a delay and a Doppler shift. This channel can be represented in delay-Doppler domain as

$$h(\tau, \nu) = \sum_{i=1}^P h_i \delta(\tau - \tau_i) \delta(\nu - \nu_i), \quad (18)$$

where  $h_i, \tau_i, \nu_i$  represent the channel gain, delay, and Doppler shift associated with  $i$ th cluster, respectively. Define  $\tau_i \triangleq \frac{\alpha_i}{M\Delta f}$  and  $\nu_i \triangleq \frac{\beta_i}{NT}$ , where  $\alpha_i$  and  $\beta_i$  denote the indices of the delay tap and Doppler frequency tap corresponding to  $\tau_i$  and  $\nu_i$ , respectively. The delay and Doppler values need not exactly be integer multiples of the taps in practice. However, sampling and discretizing the delay-Doppler plane allows us to approximate them with a few delay-Doppler taps [13]. With this assumption and assuming the transmit and receive window function  $W_{tx}[n, m]$  and  $W_{rx}[n, m]$  to be rectangular, the input-output relation for the channel in (18) can be derived as [10]

$$y[k, l] = \sum_{i=1}^P h'_i x[((k - \beta_i))_N, ((l - \alpha_i))_M] + v[k, l]. \quad (19)$$

The  $h_i$ 's are given by

$$h_i' = h_i e^{-j2\pi\nu_i\tau_i}, \quad (20)$$

where  $h_i$ 's are i.i.d and are distributed as  $\mathcal{CN}(0, 1/P)$  (assuming uniform power-delay profile). The input-output relation in (19) can be vectorized as [10]

$$\mathbf{y} = \mathbf{H}\mathbf{x} + \mathbf{v}, \quad (21)$$

where  $\mathbf{x}, \mathbf{y}, \mathbf{v} \in \mathbb{C}^{MN \times 1}$ ,  $\mathbf{H} \in \mathbb{C}^{MN \times MN}$ , the  $(k + Nl)$ th element of  $\mathbf{x}$ ,  $x_{k+Nl} = x[k, l]$ ,  $k = 0, \dots, N-1$ ,  $l = 0, \dots, M-1$ , and the same relation holds for  $\mathbf{y}$  and  $\mathbf{v}$ .

### III. DIVERSITY ANALYSIS OF OTFS

Consider the vectorized formulation of input-output relation in the SISO OTFS scheme given by (21). Note that there are only  $P$  non-zero elements in each row and column of the equivalent channel matrix ( $\mathbf{H}$ ) due to modulo operations. Hence the vectorized input-output relation in (21) can be rewritten in an alternate form as

$$\mathbf{y}^T = \mathbf{h}'\mathbf{X} + \mathbf{v}^T, \quad (22)$$

where  $\mathbf{y}^T$  is  $1 \times MN$  received vector,  $\mathbf{h}'$  is a  $1 \times P$  vector whose  $i$ th entry is given by  $h_i' = h_i e^{-j2\pi\nu_i\tau_i}$ ,  $\mathbf{v}^T$  is the  $1 \times MN$  noise vector, and  $\mathbf{X}$  is a  $P \times MN$  matrix whose  $i$ th column ( $i = k + Nl$ ,  $i = 0, 1, \dots, MN-1$ ), denoted by  $\mathbf{X}[i]$ , is given by

$$\mathbf{X}[i] = \begin{bmatrix} x_{(k-\beta_1)_N + N(l-\alpha_1)_M} \\ x_{(k-\beta_2)_N + N(l-\alpha_2)_M} \\ \vdots \\ x_{(k-\beta_P)_N + N(l-\alpha_P)_M} \end{bmatrix}. \quad (23)$$

The representation of  $\mathbf{X}$  in the form given in (22) allows us to view  $\mathbf{X}$  as a  $P \times MN$  symbol matrix. For convenience, we normalize the elements of  $\mathbf{X}$  so that the average energy per symbol time is one. The signal-to-noise ratio (SNR), denoted by  $\gamma$ , is therefore given by  $\gamma = 1/N_0$ . Assuming perfect channel state information and ML detection at the receiver, the probability of transmitting the symbol matrix  $\mathbf{X}_i$  and deciding in favor of  $\mathbf{X}_j$  at the receiver is the pairwise error probability (PEP) between  $\mathbf{X}_i$  and  $\mathbf{X}_j$ , given by [14]

$$P(\mathbf{X}_i \rightarrow \mathbf{X}_j | \mathbf{h}', \mathbf{X}_i) = Q \left( \sqrt{\frac{\|\mathbf{h}'(\mathbf{X}_i - \mathbf{X}_j)\|^2}{2N_0}} \right). \quad (24)$$

The PEP averaged over the channel statistics can be written as

$$P(\mathbf{X}_i \rightarrow \mathbf{X}_j) = \mathbb{E} \left[ Q \left( \sqrt{\frac{\gamma \|\mathbf{h}'(\mathbf{X}_i - \mathbf{X}_j)\|^2}{2}} \right) \right]. \quad (25)$$

This can be simplified by writing  $\|\mathbf{h}'(\mathbf{X}_i - \mathbf{X}_j)\|^2$  as

$$\|\mathbf{h}'(\mathbf{X}_i - \mathbf{X}_j)\|^2 = \mathbf{h}'^H (\mathbf{X}_i - \mathbf{X}_j) (\mathbf{X}_i - \mathbf{X}_j)^H \mathbf{h}'. \quad (26)$$

The matrix  $(\mathbf{X}_i - \mathbf{X}_j)(\mathbf{X}_i - \mathbf{X}_j)^H$  is Hermitian matrix that is diagonalizable by unitary transformation. Hence it can be written as

$$(\mathbf{X}_i - \mathbf{X}_j)(\mathbf{X}_i - \mathbf{X}_j)^H = \mathbf{U}\mathbf{\Lambda}\mathbf{U}^H, \quad (27)$$

where  $\mathbf{U}$  is unitary and  $\mathbf{\Lambda} = \text{diag}\{\lambda_1^2, \dots, \lambda_r^2\}$ ,  $\lambda_i$  being  $i$ th singular value of the difference matrix  $\mathbf{\Delta}_{ij}$ , given by  $\mathbf{\Delta}_{ij} = (\mathbf{X}_i - \mathbf{X}_j)$ . Substituting (27) in (26), and defining  $\tilde{\mathbf{h}} = \mathbf{U}^H \mathbf{h}'$ , (26) can be simplified as

$$\|\mathbf{h}'(\mathbf{X}_i - \mathbf{X}_j)\|^2 = \tilde{\mathbf{h}}^H \mathbf{\Lambda} \tilde{\mathbf{h}} = \sum_{l=1}^r \lambda_l^2 |\tilde{h}_l|^2, \quad (28)$$

where  $r$  denotes the rank of the difference matrix  $\mathbf{\Delta}_{ij}$ . Substituting (28) in (25), the average PEP between symbol matrices  $\mathbf{X}_i$  and  $\mathbf{X}_j$  can be written as

$$P(\mathbf{X}_i \rightarrow \mathbf{X}_j) = \mathbb{E} \left[ Q \left( \sqrt{\frac{\gamma \sum_{l=1}^r \lambda_l^2 |\tilde{h}_l|^2}{2}} \right) \right]. \quad (29)$$

Note that, since  $\tilde{\mathbf{h}}$  is obtained by multiplying a unitary matrix to  $\mathbf{h}'$ , it has the same distribution as that of  $\mathbf{h}'$ . Therefore,  $\tilde{h}_l$ 's are distributed as  $\mathcal{CN}(0, 1/P)$ . Using this, the average PEP in (29) can be simplified to get the following upper bound on PEP [14]

$$P(\mathbf{X}_i \rightarrow \mathbf{X}_j) \leq \prod_{l=1}^r \frac{1}{1 + \frac{\gamma \lambda_l^2}{4P}}. \quad (30)$$

At high SNRs, (30) can be further simplified as

$$P(\mathbf{X}_i \rightarrow \mathbf{X}_j) \leq \frac{1}{\gamma^r \prod_{l=1}^r \frac{\lambda_l^2}{4P}}. \quad (31)$$

From (31), it can be seen that the exponent of the SNR term  $\gamma$  is  $r$ , which is equal to the rank of the difference matrix  $\mathbf{\Delta}_{ij}$ . For all  $i, j$ ,  $i \neq j$ , the PEP with the minimum value of  $r$  dominates the overall BER. Therefore, the achieved diversity order, denoted by  $\rho_{\text{siso-otfs}}$ , is given by

$$\rho_{\text{siso-otfs}} = \min_{i, j, i \neq j} \text{rank}(\mathbf{\Delta}_{ij}). \quad (32)$$

Now, consider a case when  $x_i[k, l] = a$  and  $x_j[k, l] = a'$ ,  $\forall k = 0, \dots, N-1$  and  $l = 0, \dots, M-1$ . This corresponds to the case when  $\mathbf{X}_i = a \cdot \mathbf{1}_{P \times MN}$  and  $\mathbf{X}_j = a' \cdot \mathbf{1}_{P \times MN}$ . Then,  $\mathbf{\Delta}_{ij} = (\mathbf{X}_i - \mathbf{X}_j) = (a - a') \cdot \mathbf{1}_{P \times MN}$ , whose rank is one, which is the minimum rank of  $\mathbf{\Delta}_{ij}$ ,  $\forall i, j$ ,  $i \neq j$ . Hence, the asymptotic diversity order of OTFS with ML detection is one.  $\square$

From the above diversity analysis, it is evident that OTFS does not extract full diversity in the asymptotic regime and the asymptotic diversity order is equal to one. However, using a lower bound on the average BER and simulation results, we show next that, under certain conditions, OTFS can achieve close to full diversity in the finite SNR regime.

#### A. Lower bound on the average BER

In this subsection, we derive a lower bound on the BER of OTFS. This lower bound, along with simulation results in the next subsection, provides insight into finite SNR diversity of OTFS. For the ease of exposition, we assume BPSK symbols. We obtain a lower bound on BER by summing the PEPs corresponding to all the pairs  $\mathbf{X}_i$  and  $\mathbf{X}_j$ , such that the

Parameter	Value
Carrier frequency (GHz)	4
Subcarrier spacing (kHz)	3.75
Number of paths ( $P$ )	4
Delay-Doppler profile $(\tau_i, \nu_i)$	$(0, 0), (0, \frac{1}{NT}), (\frac{1}{M\Delta f}, 0), (\frac{1}{M\Delta f}, \frac{1}{NT})$
Maximum speed (km/h)	506.25
Modulation scheme	BPSK

TABLE I: Simulation parameters

difference matrix  $\Delta_{ij} = (\mathbf{X}_i - \mathbf{X}_j)$  has rank equal one. With this, a lower bound on BER is given by

$$\text{BER} \geq \frac{1}{2^{MN}} \sum_{k=1}^{\kappa} P(\mathbf{X}_i \rightarrow \mathbf{X}_j), \quad (33)$$

where  $\kappa$  denotes the number of difference matrices ( $\Delta_{ij}$ s) having rank one. When  $\Delta_{ij}$  has rank one, it has only one non-zero singular value ( $\lambda_1$ ), which can be computed to be  $\sqrt{4PMN}$ . With this, the PEP in (29), for the pair  $(\mathbf{X}_i, \mathbf{X}_j)$  with  $\Delta_{ij}$  having rank one simplifies to

$$P(\mathbf{X}_i \rightarrow \mathbf{X}_j) = \mathbb{E} \left[ Q \left( \sqrt{2\gamma PMN |\tilde{h}_1|^2} \right) \right]. \quad (34)$$

Since  $\tilde{h}_1 \sim \mathcal{CN}(0, 1/P)$ , evaluating the expectation in (34) gives [14]

$$P(\mathbf{X}_i \rightarrow \mathbf{X}_j) = \frac{1}{2} \left( 1 - \sqrt{\frac{MN}{MN + \gamma^{-1}}} \right). \quad (35)$$

Using (35) in (33), we get the lower bound as

$$\text{BER} \geq \frac{\kappa}{2^{MN}} \frac{1}{2} \left( 1 - \sqrt{\frac{MN}{MN + \gamma^{-1}}} \right). \quad (36)$$

At high SNRs, this can be further simplified as

$$\text{BER} \geq \frac{\kappa}{2^{MN}} \frac{1}{4\gamma MN}. \quad (37)$$

Observe that (37) serves as diversity one lower bound on the average BER and its value depends on the ratio  $\frac{\kappa}{2^{MN}}$ . As the values  $M$  and  $N$  increase, the  $2^{MN}$  term dominates the ratio  $\frac{\kappa}{2^{MN}}$ , and therefore increasing  $M$  and  $N$  reduces the value of the lower bound in (37). We will observe this behavior in the simulation results presented in the next subsection. Further, we will also see that the BER meets the lower bound at high SNR values. This means that the BER should decrease with a higher slope for higher values of  $M$  and  $N$  before it changes the slope and meets the diversity one lower bound of (37).

### B. Simulation results

Figure 2 shows the simulated BER performance of OTFS with  $M = 2$ ,  $N = 2$ , and BPSK. The channel model is according to (18), and the number taps is considered to be four (i.e.,  $P = 4$ ). A carrier frequency of 4 GHz and a subcarrier spacing of 3.75 kHz are considered. Other parameters considered for the simulation are given in Table

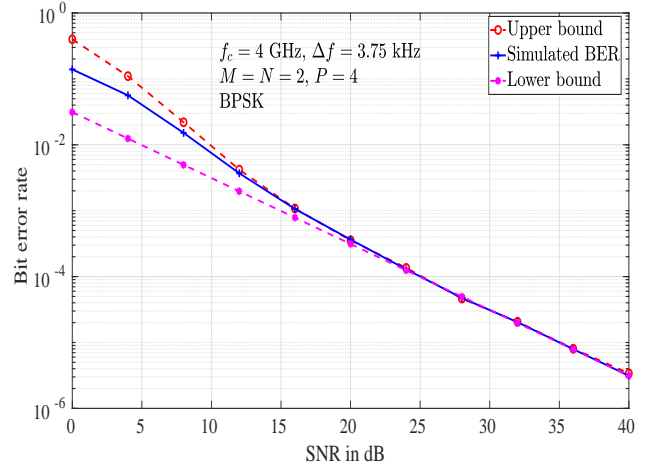


Fig. 2: Upper bound, lower bound, and the simulated BER performance of OTFS with  $M = N = 2$  and  $P = 4$ .

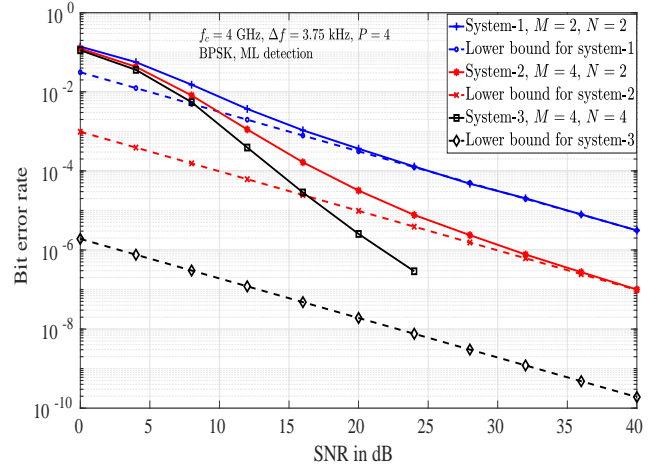


Fig. 3: BER performance of OTFS for *i*)  $M = 2$ ,  $N = 2$ , *ii*)  $M = 4$ ,  $N = 2$ , *iii*)  $M = 4$ ,  $N = 4$ .

I. In addition to the simulated BER, we have also plotted the lower bound of (37) and the union bound based upper bound for the considered system. It can be seen from the figure that the simulated BER, the lower bound, and the upper bound coincide at high SNR values, which means that the bounds are tight in the high SNR regime. Further, it can be seen that, the simulated BER shows a higher diversity order in the low to medium SNR regime, before it changes the slope and meets the diversity one lower bound.

Figure 3 shows the simulated BER performance of OTFS for different values of  $M$  and  $N$ . We consider the following three systems: *i*) system-1 with  $M = N = 2$ , *ii*) system-2 with  $M = 4$ ,  $N = 2$ , and *iii*) system-3 with  $M = N = 4$ . All the three systems use BPSK. The lower bounds given by (37) for all the three systems are also plotted. We note that the  $\frac{\kappa}{2^{MN}}$  values for the considered systems are  $\frac{8}{16}$ ,  $\frac{8}{256}$ , and  $\frac{8}{65536}$ , respectively. For illustration purposes, the  $\kappa = 8$  pairs of matrices  $(\mathbf{X}_i, \mathbf{X}_j)$  which result in rank one  $\Delta_{ij}$  matrices for the system with  $M = N = 2$  are given in Table II.

$\mathbf{X}_i$	$\mathbf{X}_j$	$\Delta_{ij} = (\mathbf{X}_i - \mathbf{X}_j)$
$\begin{bmatrix} -1 & -1 & -1 & -1 \\ -1 & -1 & -1 & -1 \\ -1 & -1 & -1 & -1 \\ -1 & -1 & -1 & -1 \end{bmatrix}$	$\begin{bmatrix} 1 & 1 & 1 & 1 \\ 1 & 1 & 1 & 1 \\ 1 & 1 & 1 & 1 \\ 1 & 1 & 1 & 1 \end{bmatrix}$	$\begin{bmatrix} -2 & -2 & -2 & -2 \\ -2 & -2 & -2 & -2 \\ -2 & -2 & -2 & -2 \\ -2 & -2 & -2 & -2 \end{bmatrix}$
$\begin{bmatrix} 1 & 1 & -1 & -1 \\ 1 & 1 & -1 & -1 \\ -1 & -1 & 1 & 1 \\ -1 & -1 & 1 & 1 \end{bmatrix}$	$\begin{bmatrix} -1 & -1 & 1 & 1 \\ -1 & -1 & 1 & 1 \\ 1 & 1 & -1 & -1 \\ 1 & 1 & -1 & -1 \end{bmatrix}$	$\begin{bmatrix} 2 & 2 & -2 & -2 \\ 2 & 2 & -2 & -2 \\ -2 & -2 & 2 & 2 \\ -2 & -2 & 2 & 2 \end{bmatrix}$
$\begin{bmatrix} -1 & 1 & 1 & -1 \\ 1 & -1 & -1 & 1 \\ 1 & -1 & -1 & 1 \\ -1 & 1 & 1 & -1 \end{bmatrix}$	$\begin{bmatrix} 1 & -1 & -1 & 1 \\ -1 & 1 & 1 & -1 \\ -1 & 1 & 1 & -1 \\ 1 & -1 & -1 & 1 \end{bmatrix}$	$\begin{bmatrix} -2 & 2 & 2 & -2 \\ 2 & -2 & -2 & 2 \\ 2 & -2 & -2 & 2 \\ -2 & 2 & 2 & -2 \end{bmatrix}$
$\begin{bmatrix} 1 & -1 & 1 & -1 \\ -1 & 1 & -1 & 1 \\ 1 & -1 & 1 & -1 \\ -1 & 1 & -1 & 1 \end{bmatrix}$	$\begin{bmatrix} -1 & 1 & -1 & 1 \\ 1 & -1 & 1 & -1 \\ -1 & 1 & -1 & 1 \\ 1 & -1 & 1 & -1 \end{bmatrix}$	$\begin{bmatrix} 2 & -2 & 2 & -2 \\ -2 & 2 & -2 & 2 \\ 2 & -2 & 2 & -2 \\ -2 & 2 & -2 & 2 \end{bmatrix}$
$\begin{bmatrix} 1 & -1 & -1 & 1 \\ -1 & 1 & 1 & -1 \\ -1 & 1 & 1 & -1 \\ 1 & -1 & -1 & 1 \end{bmatrix}$	$\begin{bmatrix} -1 & 1 & 1 & -1 \\ 1 & -1 & -1 & 1 \\ 1 & -1 & -1 & 1 \\ -1 & 1 & 1 & -1 \end{bmatrix}$	$\begin{bmatrix} 2 & -2 & -2 & 2 \\ -2 & 2 & 2 & -2 \\ -2 & 2 & 2 & -2 \\ 2 & -2 & -2 & 2 \end{bmatrix}$
$\begin{bmatrix} -1 & 1 & -1 & 1 \\ 1 & -1 & 1 & -1 \\ -1 & 1 & -1 & 1 \\ 1 & -1 & 1 & -1 \end{bmatrix}$	$\begin{bmatrix} 1 & -1 & 1 & -1 \\ -1 & 1 & -1 & 1 \\ 1 & -1 & 1 & -1 \\ -1 & 1 & -1 & 1 \end{bmatrix}$	$\begin{bmatrix} -2 & 2 & -2 & 2 \\ 2 & -2 & 2 & -2 \\ -2 & 2 & -2 & 2 \\ 2 & -2 & 2 & -2 \end{bmatrix}$
$\begin{bmatrix} -1 & -1 & 1 & 1 \\ -1 & -1 & 1 & 1 \\ 1 & 1 & -1 & -1 \\ 1 & 1 & -1 & -1 \end{bmatrix}$	$\begin{bmatrix} 1 & 1 & -1 & -1 \\ 1 & 1 & -1 & -1 \\ -1 & -1 & 1 & 1 \\ -1 & -1 & 1 & 1 \end{bmatrix}$	$\begin{bmatrix} -2 & -2 & 2 & 2 \\ -2 & -2 & 2 & 2 \\ 2 & 2 & -2 & -2 \\ 2 & 2 & -2 & -2 \end{bmatrix}$
$\begin{bmatrix} 1 & 1 & 1 & 1 \\ 1 & 1 & 1 & 1 \\ 1 & 1 & 1 & 1 \\ 1 & 1 & 1 & 1 \end{bmatrix}$	$\begin{bmatrix} -1 & -1 & -1 & -1 \\ -1 & -1 & -1 & -1 \\ -1 & -1 & -1 & -1 \\ -1 & -1 & -1 & -1 \end{bmatrix}$	$\begin{bmatrix} 2 & 2 & 2 & 2 \\ 2 & 2 & 2 & 2 \\ 2 & 2 & 2 & 2 \\ 2 & 2 & 2 & 2 \end{bmatrix}$

TABLE II: The pair of matrices  $(\mathbf{X}_i, \mathbf{X}_j)$  and the corresponding  $\Delta_{ij}$  with rank equal to one in OTFS with  $M = N = 2$ .

Since the  $\frac{\kappa}{2^{MN}}$  values are decreasing for increasing  $MN$ , (37) indicates that the lower bound for system-3 should lie below that of system-2, which, in turn, should lie below that of system-1. This trend is clearly evident from Fig. 3. Further, as noted before, for all the systems, the BER plots show a diversity order greater than one for low to medium SNR values before it meets the diversity one lower bound. An interesting observation, however, is that the system-3 with higher  $M$  and  $N$  values achieves a higher diversity order compared to those of systems-1 and 2 before meeting the lower bound. This is because the lower bound for system-3 lies much below the lower bounds for systems-1 and 2, and the BER curve of system-3 falls with greater slope to meet its lower bound. This shows that, though the asymptotic diversity order is one, increasing the value of  $MN$  (i.e., increasing the frame size) can lead to higher diversity order in the finite SNR regime, resulting in improved performance for increased frame sizes.

#### IV. PHASE ROTATION FOR FULL DIVERSITY IN OTFS

In the previous section, we showed that the asymptotic diversity of OTFS is one, and that potential for higher diversity orders is observed in the finite SNR regime for large frame sizes before the diversity one regime takes over. In this section, we propose a ‘phase rotation’ scheme which extracts the full diversity offered by the delay-Doppler channel. From the diversity analysis in Sec. III, it is clear that the asymptotic diversity order of OTFS depends on the minimum rank of the difference matrix  $\Delta_{ij} = (\mathbf{X}_i - \mathbf{X}_j)$ , over all pairs of symbol

matrices  $(\mathbf{X}_i, \mathbf{X}_j)$ . In order to design a scheme that can extract full diversity, we take a closer look at the symbol matrix  $\mathbf{X}$  whose  $i$ th column is given by (23). The symbol matrix  $\mathbf{X}$  is a  $P \times MN$  matrix that has only  $MN$  unique entries, which are nothing but the  $MN$  symbols of the transmit vector  $\mathbf{x}$ . The rows of the matrix  $\mathbf{X}$  are the permutations of the transmit symbol vector  $\mathbf{x}$ . When  $P = MN$ , the matrix  $\mathbf{X}$  is a block circulant matrix with circulant blocks, as shown in (38). Note that  $\mathbf{X}$  has  $M$  circulant blocks, each of size  $N \times N$ , which are cyclically shifted to form a block circulant matrix. In (38),  $x_q^{(l)}$  denotes the  $q$ th distinct element of the  $l$ th block, where  $q = 0, \dots, N-1$  and  $l = 0, \dots, M-1$ . When  $P < MN$ , the  $P$  rows of the matrix  $\mathbf{X}$  are a subset of rows from (38), and the selected subset depends on the positions of non-zero entries in the delay-Doppler channel matrix. This structure of  $\mathbf{X}$  arises naturally from OTFS pre- and post-processing operations (ISFFT and SFFT) which result in the 2D circular convolution of the transmit vector  $\mathbf{x}$  with the channel response in delay-Doppler domain.

The  $MN \times 1$  OTFS transmit vector corresponding to the symbol matrix  $\mathbf{X}$  in (38) is given by

$$\mathbf{x} = [x_0^{(0)}, \dots, x_{N-1}^{(0)}, x_0^{(1)}, \dots, x_{N-1}^{(1)}, \dots, x_{N-1}^{(M-1)}]^T. \quad (39)$$

The following theorem shows that multiplying the OTFS transmit vector in (39) by a diagonal phase rotation matrix  $\Phi$  with distinct transcendental numbers results in full diversity.

$$\mathbf{X} = \begin{bmatrix} \begin{array}{cccc|cccc|c} x_0^{(0)} & x_1^{(0)} & \cdots & x_{N-1}^{(0)} & x_0^{(1)} & x_1^{(1)} & \cdots & x_{N-1}^{(1)} & \dots \\ x_{N-1}^{(0)} & x_0^{(0)} & \cdots & x_{N-2}^{(0)} & x_{N-1}^{(1)} & x_0^{(1)} & \cdots & x_{N-2}^{(1)} & \dots \\ & & \vdots & & & & \vdots & & \\ x_1^{(0)} & x_2^{(0)} & \cdots & x_0^{(0)} & x_1^{(1)} & x_2^{(1)} & \cdots & x_0^{(1)} & \dots \\ \hline x_0^{(M-1)} & x_1^{(M-1)} & \cdots & x_{N-1}^{(M-1)} & x_0^{(0)} & x_1^{(0)} & \cdots & x_{N-1}^{(0)} & \dots \\ x_{N-1}^{(M-1)} & x_0^{(M-1)} & \cdots & x_{N-2}^{(M-1)} & x_{N-1}^{(0)} & x_0^{(0)} & \cdots & x_{N-2}^{(0)} & \dots \\ & & \vdots & & & & \vdots & & \\ x_1^{(M-1)} & x_2^{(M-1)} & \cdots & x_0^{(M-1)} & x_1^{(0)} & x_2^{(0)} & \cdots & x_0^{(0)} & \dots \\ \hline & \vdots & & & & \vdots & & & \\ \hline & & & & x_0^{(2)} & x_1^{(2)} & \cdots & x_{N-1}^{(2)} & \dots \\ & & & & x_{N-1}^{(2)} & x_0^{(2)} & \cdots & x_{N-2}^{(2)} & \dots \\ & & & & & & \vdots & & \\ & & & & x_1^{(2)} & x_2^{(2)} & \cdots & x_0^{(2)} & \dots \end{array} & \begin{array}{cccc|cccc|c} x_0^{(M-1)} & x_1^{(M-1)} & \cdots & x_{N-1}^{(M-1)} & x_0^{(0)} & x_1^{(0)} & \cdots & x_{N-1}^{(0)} & \dots \\ x_{N-1}^{(M-1)} & x_0^{(M-1)} & \cdots & x_{N-2}^{(M-1)} & x_{N-1}^{(0)} & x_0^{(0)} & \cdots & x_{N-2}^{(0)} & \dots \\ & & \vdots & & & & \vdots & & \\ x_1^{(M-1)} & x_2^{(M-1)} & \cdots & x_0^{(M-1)} & x_1^{(0)} & x_2^{(0)} & \cdots & x_0^{(0)} & \dots \\ \hline & \vdots & & & & \vdots & & & \\ \hline & & & & x_0^{(0)} & x_1^{(0)} & \cdots & x_{N-1}^{(0)} & \dots \\ & & & & x_{N-1}^{(0)} & x_0^{(0)} & \cdots & x_{N-2}^{(0)} & \dots \\ & & & & & & \vdots & & \\ & & & & x_1^{(0)} & x_2^{(0)} & \cdots & x_0^{(0)} & \dots \end{array} \end{bmatrix}. \quad (38)$$

**Theorem 1. Let**

$$\Phi = \text{diag} \left\{ \phi_0^{(0)}, \dots, \phi_{N-1}^{(0)}, \phi_0^{(1)}, \dots, \phi_{N-1}^{(1)}, \dots, \phi_{N-1}^{(M-1)} \right\} \quad (40)$$

be the phase rotation matrix and

$$\mathbf{x}' = \Phi \mathbf{x} = \begin{bmatrix} \phi_0^{(0)} x_0^{(0)} \\ \vdots \\ \phi_{N-1}^{(0)} x_{N-1}^{(0)} \\ \phi_0^{(1)} x_0^{(1)} \\ \vdots \\ \phi_{N-1}^{(1)} x_{N-1}^{(1)} \\ \vdots \\ \phi_{N-1}^{(M-1)} x_{N-1}^{(M-1)} \end{bmatrix} \quad (41)$$

be the phase rotated OTFS transmit vector. OTFS with the above phase rotation achieves the full diversity of  $P$  when  $\phi_q^{(l)} = e^{ja_q^{(l)}}$ ,  $q = 0, \dots, N-1$ ,  $l = 0, \dots, M-1$  are transcendental numbers with  $a_q^{(l)} \neq 0$ , real, distinct and algebraic.

*Proof.* Let  $\mathbf{x}'_i = \Phi \mathbf{x}_i$  and  $\mathbf{x}'_j = \Phi \mathbf{x}_j$  be two phase rotated OTFS transmit vectors. Let  $\mathbf{X}'_i$  and  $\mathbf{X}'_j$  denote the corresponding phase rotated symbol matrices.

Case 1:  $P = MN$

When  $P = MN$ , the symbol matrices  $\mathbf{X}'_i$  and  $\mathbf{X}'_j$  are block circulant with circulant blocks, and hence  $\Delta'_{ij} = \mathbf{X}'_i - \mathbf{X}'_j$  also has the same structure, i.e.,

$$\Delta'_{ij} = \begin{bmatrix} \Delta'_{ij}{}^{(0)} & \Delta'_{ij}{}^{(1)} & \cdots & \Delta'_{ij}{}^{(M-1)} \\ \Delta'_{ij}{}^{(M-1)} & \Delta'_{ij}{}^{(0)} & \cdots & \Delta'_{ij}{}^{(M-2)} \\ \vdots & \vdots & \vdots & \vdots \\ \Delta'_{ij}{}^{(1)} & \Delta'_{ij}{}^{(2)} & \cdots & \Delta'_{ij}{}^{(0)} \end{bmatrix}, \quad (42)$$

where

$$\Delta'_{ij}{}^{(l)} = \begin{bmatrix} \delta_0^{(l)} \phi_0^{(l)} & \delta_1^{(l)} \phi_1^{(l)} & \cdots & \delta_{N-1}^{(l)} \phi_{N-1}^{(l)} \\ \delta_{N-1}^{(l)} \phi_{N-1}^{(l)} & \delta_0^{(l)} \phi_0^{(l)} & \cdots & \delta_{N-2}^{(l)} \phi_{N-2}^{(l)} \\ \vdots & \vdots & \ddots & \vdots \\ \delta_1^{(l)} \phi_1^{(l)} & \delta_2^{(l)} \phi_2^{(l)} & \cdots & \delta_0^{(l)} \phi_0^{(l)} \end{bmatrix}, \quad (43)$$

where  $\delta_q^{(l)} = x_{i,q}^{(l)} - x_{j,q}^{(l)}$ , with  $x_{i,q}^{(l)}$  and  $x_{j,q}^{(l)}$  being  $q$ th distinct elements in the  $l$ th block of  $\mathbf{X}_i$  and  $\mathbf{X}_j$ , respectively. Since  $\Delta'_{ij}$  is block circulant with circulant blocks, it is diagonalized by  $\mathbf{F}_M \otimes \mathbf{F}_N$ , where  $\mathbf{F}_M$  and  $\mathbf{F}_N$  denote the  $M \times M$  and  $N \times N$  DFT matrices and  $\otimes$  denotes the Kronecker product. Therefore,  $\Delta'_{ij}$  is given by [15]

$$\Delta'_{ij} = (\mathbf{F}_M \otimes \mathbf{F}_N)^H \mathbf{D} (\mathbf{F}_M \otimes \mathbf{F}_N), \quad (44)$$

where  $\mathbf{D}$  is an  $MN \times MN$  diagonal matrix whose entries are the eigen values of  $\Delta'_{ij}$ , given by

$$\mathbf{D} = \sum_{l=0}^{M-1} \Omega_M^l \otimes \Lambda^{(l)}, \quad (45)$$

where  $\Omega_M = \text{diag}\{1, \omega, \omega^2, \dots, \omega^{M-1}\}$  with  $\omega = e^{j2\pi/M}$ , and  $\Lambda^{(l)}$  is a diagonal matrix whose entries are the eigen values of  $\Delta'_{ij}{}^{(l)}$ . Let  $\lambda_q^{(l)}$  denote the  $q$ th eigen value of  $\Delta'_{ij}{}^{(l)}$  and  $\mu_0, \mu_1, \dots, \mu_{MN-1}$  denote the eigen values of  $\Delta'_{ij}$ . From (45), the  $k$ th eigen value of  $\Delta'_{ij}$ , that is,  $\mu_k$  is given by

$$\mu_k = \sum_{l=0}^{M-1} \lambda_u^{(l)} \omega^{vl}, \quad (46)$$

where  $u = k - \lfloor \frac{k}{M} \rfloor (N-1)$ ,  $v = \lfloor \frac{k}{M} \rfloor$ , and  $\lambda_u^{(l)}$  is the  $u$ th eigen value of  $\Delta'_{ij}{}^{(l)}$ , given by

$$\lambda_u^{(l)} = \sum_{q=0}^{N-1} \phi_q^{(l)} \delta_q^{(l)} e^{-j2\pi uq/N}. \quad (47)$$

Using (47) in (46), we have

$$\begin{aligned} \mu_k &= \sum_{l=0}^{M-1} \sum_{q=0}^{N-1} \phi_q^{(l)} \delta_q^{(l)} e^{-j2\pi uq/N} \omega^{vl} \\ &= \sum_{l=0}^{M-1} \left\{ \phi_0^{(l)} \delta_0^{(l)} + \phi_1^{(l)} \delta_1^{(l)} e^{-j2\pi u/N} + \right. \\ &\quad \left. \cdots + \phi_{N-1}^{(l)} \delta_{N-1}^{(l)} e^{-j2\pi u(N-1)/N} \right\} \omega^{vl}, \end{aligned} \quad (48)$$

which can be further simplified as

$$\begin{aligned} \mu_k &= \phi_0^{(0)} \delta_0^{(0)} + \phi_1^{(0)} \delta_1^{(0)} e^{-\frac{j2\pi u}{N}} + \cdots + \phi_{N-1}^{(0)} \delta_{N-1}^{(0)} e^{-\frac{j2\pi u(N-1)}{N}} \\ &\quad + \phi_0^{(1)} \delta_0^{(1)} \omega^v + \cdots + \phi_{N-1}^{(1)} \delta_{N-1}^{(1)} e^{-\frac{j2\pi u(N-1)}{N}} \omega^v + \cdots \\ &\quad + \phi_0^{(M-1)} \delta_0^{(M-1)} \omega^{v(M-1)} + \cdots \\ &\quad + \phi_{N-1}^{(M-1)} \delta_{N-1}^{(M-1)} e^{-\frac{j2\pi u(N-1)}{N}} \omega^{v(M-1)}. \end{aligned} \quad (50)$$

At this stage, we invoke the Lindenmann's theorem [16], which states that, if  $a_1, a_2, \dots, a_m$  are distinct algebraic numbers, and if  $c_1, c_2, \dots, c_m$  are algebraic and not all equal to zero, then

$$c_1 e^{a_1} + c_2 e^{a_2} + \cdots + c_m e^{a_m} \neq 0. \quad (51)$$

It should be noted from (50) that the terms of the form  $\delta_q^{(l)} e^{-\frac{j2\pi uq}{N}} \omega^{vl}$  are all algebraic [16]. Therefore, comparing (51) and (50), if the terms  $\phi_q^{(l)}$  are chosen such that  $\phi_q^{(l)} = e^{ja_q^{(l)}}$  are transcendental with  $a_q^{(l)} \neq 0$ , real, distinct and algebraic, then  $\mu_k$  can not be zero. Since  $\mu_k$ s are eigen values of  $\Delta'_{ij}$ , choosing the diagonal phase rotation matrix with entries  $\phi_q^{(l)} = e^{ja_q^{(l)}}$  being transcendental with  $a_q^{(l)} \neq 0$ , real, distinct and algebraic ensures that all the eigen values of  $\Delta'_{ij}$  are non-zero, making it full rank (i.e., rank  $P$ ). Since this is true for  $\Delta'_{ij}$  for all  $(i, j)$ ,  $i \neq j$ , the minimum rank of  $\Delta'_{ij}$  is equal to  $MN$ . Hence, from (32), the achieved diversity order of OTFS with the proposed phase rotation is  $MN$ .

*Case 2:  $P < MN$*

Now, consider the case when  $P < MN$ . As mentioned previously, when  $P < MN$ , the rows of the transmit symbol matrix  $\mathbf{X}$  is the subset of rows from the corresponding  $MN \times MN$  matrix in (38). If  $\mathbf{X}'_i$  and  $\mathbf{X}'_j$  are two phase rotated symbol matrices with  $P < MN$ , then the rows of  $\Delta'_{ij} = \mathbf{X}'_i - \mathbf{X}'_j$  form a subset of the rows of the corresponding  $MN \times MN$  matrix in (42). Since the matrix in (42) is shown to be full rank in *Case 1*,  $\Delta'_{ij}$  with  $P < MN$  should have a rank equal to  $P$ . Therefore, OTFS with phase rotation using transcendental numbers of the form  $\phi_q^{(l)} = e^{ja_q^{(l)}}$  with  $a_q^{(l)} \neq 0$ , real, distinct and algebraic achieves the full diversity of  $P$  in the delay-Doppler domain.  $\square$

### A. Simulation results

In Fig. 4, we present the simulated BER performance of OTFS with and without phase rotation for a system with  $M = N = 2$  and BPSK. The carrier frequency and the subcarrier spacing used are 4 GHz and 3.75 kHz, respectively. Other simulation parameters are as given in Table I. Figure 5 shows

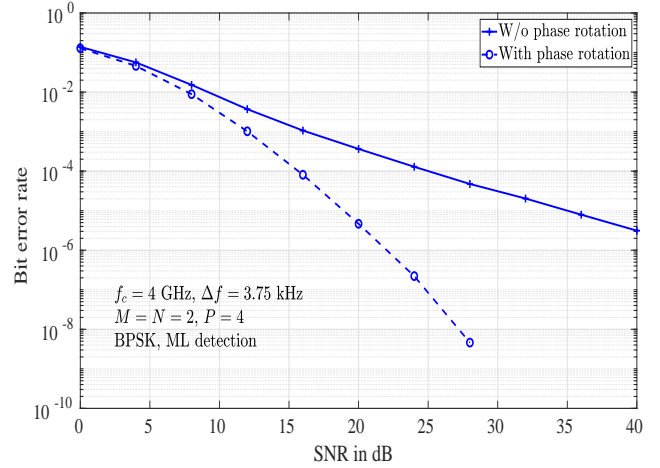


Fig. 4: BER performance of OTFS without and with phase rotation,  $M = N = 2$ , and BPSK.

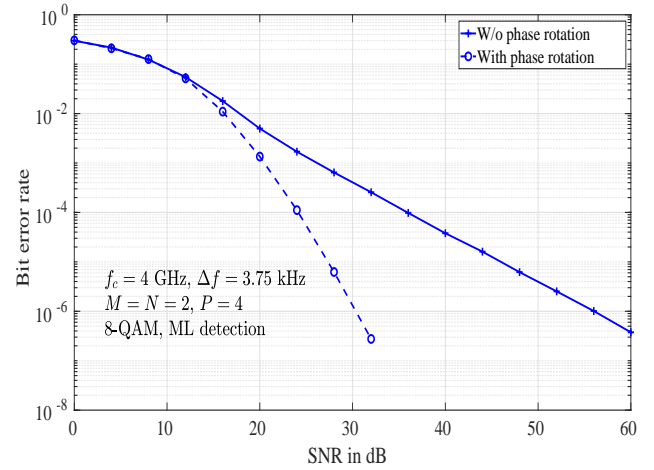


Fig. 5: BER performance of OTFS without and with phase rotation,  $M = N = 2$ , and 8-QAM.

the performance without and with phase rotation with 8-QAM. From these figures, we observe that while OTFS without phase rotation achieves a diversity order of one, OTFS with phase rotation shows the intended diversity benefit. For example, at a BER of  $10^{-5}$ , the OTFS system with phase rotation achieves an SNR gain of about 17 dB compared to the system without phase rotation.

## V. MIMO-OTFS MODULATION

In this section, we consider OTFS modulation and its diversity order in a MIMO setting.

### A. MIMO-OTFS system model

Consider a MIMO-OTFS system shown in Fig. 6 with  $n_t$  transmit and  $n_r$  receive antennas. Each antenna transmits an independent OTFS signal vector. The channel gain between the  $k$ th transmit antenna and  $l$ th receive antenna in the delay-

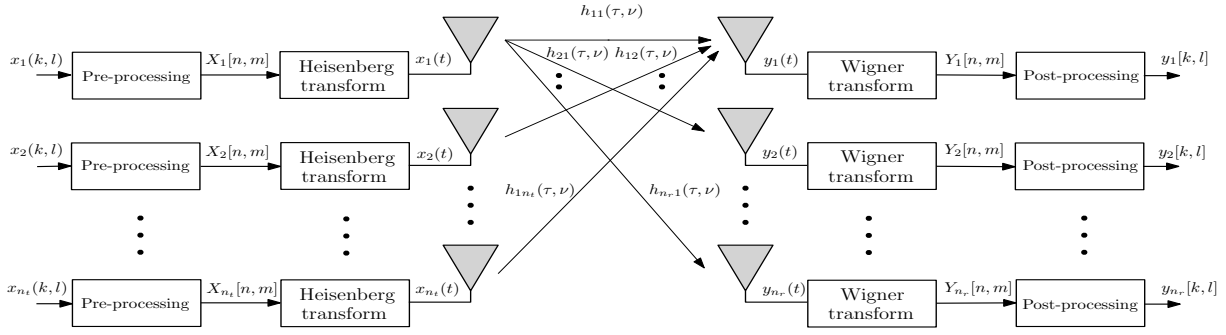


Fig. 6: MIMO-OTFS modulation scheme.

Doppler domain corresponding to delay  $\tau$  and Doppler  $\nu$  is given by

$$h_{lk}(\tau, \nu) = \sum_{i=1}^P h_{lk_i} \delta(\tau - \tau_i) \delta(\nu - \nu_i), \quad (52)$$

$k = 1, 2, \dots, n_t$ ,  $l = 1, 2, \dots, n_r$ , and  $P$  is the number of channel taps. Let  $\mathbf{H}_{lk}$  denote the  $MN \times MN$  equivalent channel matrix between the  $k$ th transmit antenna and  $l$ th receive antenna. Let  $\mathbf{x}_k$  denote the  $MN \times 1$  transmit vector from the  $k$ th transmit antenna and  $\mathbf{y}_l$  denote the  $MN \times 1$  received vector at the  $l$ th receive antenna. Then, using the linear vector channel model in (21) for SISO-OTFS, the linear system model describing the input and output relation in MIMO-OTFS can be obtained as

$$\begin{aligned} \mathbf{y}_1 &= \mathbf{H}_{11}\mathbf{x}_1 + \mathbf{H}_{12}\mathbf{x}_2 + \dots + \mathbf{H}_{1n_t}\mathbf{x}_{n_t} + \mathbf{v}_1, \\ \mathbf{y}_2 &= \mathbf{H}_{21}\mathbf{x}_1 + \mathbf{H}_{22}\mathbf{x}_2 + \dots + \mathbf{H}_{2n_t}\mathbf{x}_{n_t} + \mathbf{v}_2, \\ &\vdots \\ \mathbf{y}_{n_r} &= \mathbf{H}_{n_r,1}\mathbf{x}_1 + \mathbf{H}_{n_r,2}\mathbf{x}_2 + \dots + \mathbf{H}_{n_r,n_t}\mathbf{x}_{n_t} + \mathbf{v}_{n_r}. \end{aligned} \quad (53)$$

Defining

$$\mathbf{H}_{\text{MIMO}} = \begin{bmatrix} \mathbf{H}_{11} & \mathbf{H}_{12} & \dots & \mathbf{H}_{1n_t} \\ \mathbf{H}_{21} & \mathbf{H}_{22} & \dots & \mathbf{H}_{2n_t} \\ \vdots & \vdots & \ddots & \vdots \\ \mathbf{H}_{n_r,1} & \mathbf{H}_{n_r,2} & \dots & \mathbf{H}_{n_r,n_t} \end{bmatrix},$$

$$\mathbf{x}_{\text{MIMO}} = [\mathbf{x}_1^T, \mathbf{x}_2^T, \dots, \mathbf{x}_{n_t}^T]^T, \mathbf{y}_{\text{MIMO}} = [\mathbf{y}_1^T, \mathbf{y}_2^T, \dots, \mathbf{y}_{n_r}^T]^T, \mathbf{v}_{\text{MIMO}} = [\mathbf{v}_1^T, \mathbf{v}_2^T, \dots, \mathbf{v}_{n_r}^T]^T, \quad (53) \text{ can be written as}$$

$$\mathbf{y}_{\text{MIMO}} = \mathbf{H}_{\text{MIMO}}\mathbf{x}_{\text{MIMO}} + \mathbf{v}_{\text{MIMO}}, \quad (54)$$

where  $\mathbf{x}_{\text{MIMO}} \in \mathbb{C}^{n_t MN \times 1}$ ,  $\mathbf{y}_{\text{MIMO}}, \mathbf{v}_{\text{MIMO}} \in \mathbb{C}^{n_r MN \times 1}$ , and  $\mathbf{H}_{\text{MIMO}} \in \mathbb{C}^{n_r MN \times n_t MN}$ .

### B. Diversity of MIMO-OTFS

In this subsection, we derive the asymptotic diversity order of MIMO-OTFS. For this, first note that, in the effective channel matrix  $\mathbf{H}_{\text{MIMO}}$ , each  $\mathbf{H}_{lk}$  has only  $P$  unique entries, and hence  $\mathbf{H}_{\text{MIMO}}$  has  $Pn_t n_r$  unique entries. Further, each row of  $\mathbf{H}_{\text{MIMO}}$  has only  $n_t P$  non-zero elements and each column

has only  $n_r P$  non-zero elements. Following (22), the MIMO-OTFS system model in (54) can be written as

$$\begin{bmatrix} \mathbf{y}_1^T \\ \mathbf{y}_2^T \\ \vdots \\ \mathbf{y}_{n_r}^T \end{bmatrix} = \begin{bmatrix} \mathbf{h}'_{11} & \mathbf{h}'_{12} \cdots \mathbf{h}'_{1n_t} \\ \mathbf{h}'_{21} & \mathbf{h}'_{22} \cdots \mathbf{h}'_{2n_t} \\ \vdots & \vdots \\ \mathbf{h}'_{n_r,1} & \mathbf{h}'_{n_r,2} \cdots \mathbf{h}'_{n_r,n_t} \end{bmatrix} \begin{bmatrix} \mathbf{X}_1 \\ \mathbf{X}_2 \\ \vdots \\ \mathbf{X}_{n_t} \end{bmatrix} + \begin{bmatrix} \mathbf{v}_1^T \\ \mathbf{v}_2^T \\ \vdots \\ \mathbf{v}_{n_r}^T \end{bmatrix}, \quad (55)$$

or equivalently

$$\tilde{\mathbf{y}} = \tilde{\mathbf{H}}\tilde{\mathbf{X}} + \tilde{\mathbf{V}}, \quad (56)$$

where  $\tilde{\mathbf{y}}$  is an  $n_r \times MN$  received signal matrix whose  $l$ th row is the received vector received in the  $l$ th receive antenna,  $\tilde{\mathbf{X}}$  is an  $n_t P \times MN$  matrix obtained by stacking  $n_t$  number of  $P \times MN$  sized symbol matrices of the form (23),  $\tilde{\mathbf{H}} \in \mathbb{C}^{n_r \times n_t P}$  is the channel matrix with  $\mathbf{h}'_{lk} \in \mathbb{C}^{1 \times P}$  consisting of  $P$  unique non-zero entries of  $\mathbf{H}_{lk}$ , and  $\tilde{\mathbf{V}} \in \mathbb{C}^{n_r \times MN}$  is the noise matrix.

Let  $\tilde{\mathbf{X}}_i$  and  $\tilde{\mathbf{X}}_j$  be two symbol matrices. Assuming perfect channel state information and ML detection at the receiver, the probability of decoding the transmitted symbol matrix  $\tilde{\mathbf{X}}_i$  in favor of  $\tilde{\mathbf{X}}_j$  is given by

$$P(\tilde{\mathbf{X}}_i \rightarrow \tilde{\mathbf{X}}_j | \tilde{\mathbf{H}}) = Q \left( \sqrt{\frac{\|\tilde{\mathbf{H}}(\tilde{\mathbf{X}}_i - \tilde{\mathbf{X}}_j)\|^2}{2N_0}} \right), \quad (57)$$

and the average PEP is given by

$$P(\tilde{\mathbf{X}}_i \rightarrow \tilde{\mathbf{X}}_j) = \mathbb{E} \left[ Q \left( \sqrt{\frac{\|\tilde{\mathbf{H}}(\tilde{\mathbf{X}}_i - \tilde{\mathbf{X}}_j)\|^2}{2N_0}} \right) \right]. \quad (58)$$

Using Chernoff bound and the fact that each antenna transmits independent OTFS symbols, an upper bound on the PEP in (58) can be obtained as [14]

$$P(\tilde{\mathbf{X}}_i \rightarrow \tilde{\mathbf{X}}_j) \leq \left( \prod_{l=1}^r \frac{1}{1 + \frac{\gamma \lambda_{k,l}^2}{4P}} \right)^{n_r}, \quad (59)$$

where  $\gamma = \frac{1}{N_0}$  is the SNR per receive antenna,  $\lambda_{k,l}$  is the  $l$ th singular value of the difference matrix  $\Delta_{k,i,j} = (\mathbf{X}_{k,i} - \mathbf{X}_{k,j})$  with  $\mathbf{X}_{k,i}$  and  $\mathbf{X}_{k,j}$  denoting OTFS symbol matrices transmitted from  $k$ th antenna (for some  $k \in 1, 2, \dots, n_t$ ) in

$\tilde{\mathbf{X}}_i$  and  $\tilde{\mathbf{X}}_j$ , respectively, and  $r$  is the rank of  $\Delta_{k,ij}$ . At high SNR values, (59) simplifies to

$$P(\tilde{\mathbf{X}}_i \rightarrow \tilde{\mathbf{X}}_j) \leq \frac{1}{\gamma^{n_r r}} \left( \prod_{l=1}^r \frac{\lambda_{k,l}^2}{4P} \right)^{-n_r}. \quad (60)$$

The PEP term with the minimum value of  $r$  dominates the overall BER. Therefore, the diversity order achieved by MIMO-OTFS, denoted by  $\rho_{\text{mimo-otfs}}$  is given by

$$\rho_{\text{mimo-otfs}} = n_r \cdot \min_{i,j, i \neq j} \text{rank}(\Delta_{k,ij}). \quad (61)$$

Now, similar to the case of SISO-OTFS, if  $\mathbf{X}_{k,i} = a \cdot \mathbf{1}_{P \times MN}$  and  $\mathbf{X}_{k,j} = a' \cdot \mathbf{1}_{P \times MN}$ , then the difference matrix  $\Delta_{k,ij} = (a - a') \cdot \mathbf{1}_{P \times MN}$  has rank one. Hence, the asymptotic diversity order of MIMO-OTFS is  $n_r$ .  $\square$

### C. Phase rotation for full diversity in MIMO-OTFS

In this subsection, we consider phase rotation to extract the full diversity in MIMO-OTFS. The transmit vector in MIMO-OTFS is a concatenation of  $n_t$  independent OTFS transmit vectors of size  $MN \times 1$  as described by (54). The  $MN \times 1$  OTFS transmit vector from each antenna is multiplied by the phase rotation matrix  $\Phi$  given in (40). The phase rotated MIMO-OTFS transmit vector is then given by

$$\mathbf{x}'_{\text{MIMO}} = (\mathbf{I}_{n_t} \otimes \Phi) \mathbf{x}_{\text{MIMO}}. \quad (62)$$

Let  $\tilde{\mathbf{X}}'$  be the phase rotated MIMO-OTFS symbol matrix corresponding to  $\mathbf{x}'$ . From (55),  $\tilde{\mathbf{X}}'$  is of the form

$$\tilde{\mathbf{X}}' = \begin{bmatrix} \mathbf{X}'_1 \\ \mathbf{X}'_2 \\ \vdots \\ \mathbf{X}'_{n_t} \end{bmatrix}, \quad (63)$$

where  $\mathbf{X}'_k$  is the phase rotated OTFS symbol matrix corresponding to the  $k$ th transmit antenna. If  $\tilde{\mathbf{X}}'_i$  and  $\tilde{\mathbf{X}}'_j$  are two phase rotated MIMO-OTFS symbol matrices corresponding to the transmit vectors  $\mathbf{x}'_{i,\text{MIMO}}$  and  $\mathbf{x}'_{j,\text{MIMO}}$ , then their difference matrix  $\tilde{\Delta}'_{ij}$  is of the form

$$\tilde{\Delta}'_{ij} = \begin{bmatrix} \Delta'_{1,ij} \\ \Delta'_{2,ij} \\ \vdots \\ \Delta'_{n_t,ij} \end{bmatrix}, \quad (64)$$

where  $\Delta'_{k,ij} = \mathbf{X}'_{k,i} - \mathbf{X}'_{k,j}$ , with  $\mathbf{X}'_{k,i}$  and  $\mathbf{X}'_{k,j}$  being the phase rotated OTFS symbol matrices corresponding to the  $k$ th antenna in  $\tilde{\mathbf{X}}'_i$  and  $\tilde{\mathbf{X}}'_j$ , respectively. From Sec. IV, it is known that  $\Delta'_{k,ij}$  has rank equal to  $P$  for all  $k = 1, 2, \dots, n_t$ . Using this fact in (61), the diversity order achieved by phase rotated MIMO-OTFS system is equal to  $Pn_r$ .  $\square$

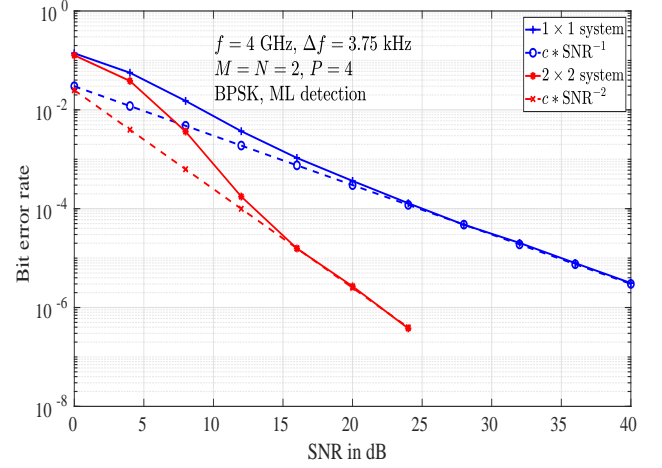


Fig. 7: BER performance of  $1 \times 1$  SISO-OTFS and  $2 \times 2$  MIMO-OTFS systems.

### D. Simulation results

Figure 7 shows the BER performance of  $1 \times 1$  SISO-OTFS and  $2 \times 2$  MIMO-OTFS systems. Both the systems use  $M = N = 2$  and BPSK. The number of channel taps considered is  $P = 4$ . The carrier frequency and the subcarrier spacing used are 4 GHz and 3.75 kHz, respectively. The considered simulation parameters are summarized in Table I. From the figure, it is observed that the simulated BER for  $1 \times 1$  SISO-OTFS and  $2 \times 2$  MIMO-OTFS systems show diversity orders of one and two, respectively, verifying the analytical diversity order derived in the previous subsection.

Next, we consider the effect of increasing the frame size (i.e.,  $MN$ ) on the BER performance. Figure 8 shows the BER performance of  $1 \times 2$  system with *i*)  $M = N = 2$  and *ii*)  $M = 4, N = 2$ . Both the systems use BPSK. The number of channel taps considered is  $P = 4$ . Other simulation parameters are as given in Table I. From the figure, we observe that the BER performance of the system with  $M = 4$  and  $N = 2$  is better than the system with  $M = N = 2$ . This is similar to the SISO-OTFS result shown in Sec. III-B. Specifically, increasing the frame size ( $MN$ ) results in higher diversity order in the finite SNR regime, before the asymptotic diversity order of  $\rho_{\text{mimo-otfs}} = 2$  takes over. It can be observed that, MIMO-OTFS can achieve diversity orders closer to  $Pn_r$  in the finite SNR regime, as the size of the OTFS frame  $MN$  is increased.

Figure 9 shows the BER performance of a  $2 \times 2$  MIMO-OTFS systems with and without phase rotation with  $M = N = 2$  and BPSK. From the figure, it can be seen that the MIMO-OTFS system with phase rotation achieves the intended diversity benefit compared to the diversity in MIMO-OTFS without phase rotation.

## VI. CONCLUSIONS

We investigated the diversity of OTFS modulation and showed that the asymptotic diversity order of OTFS in a SISO setting with ML detection is one. Though the asymptotic

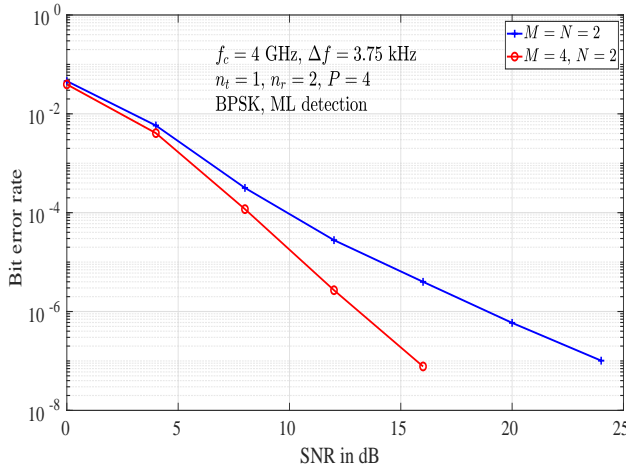


Fig. 8: BER performance of  $1 \times 2$  OTFS system with *i)*  $M = N = 2$  and *ii)*  $M = 4, N = 2$ .

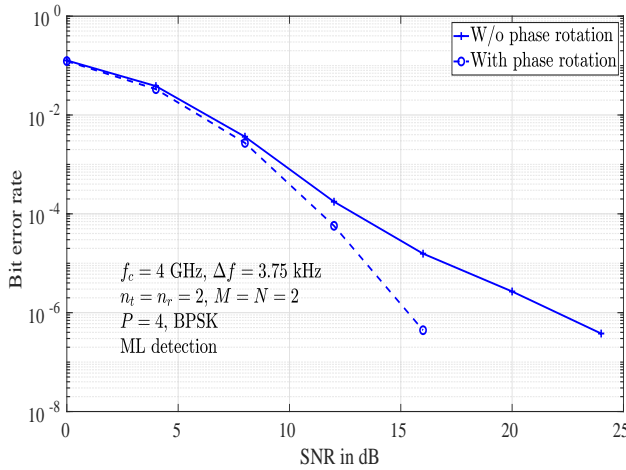


Fig. 9: BER performance of  $2 \times 2$  MIMO-OTFS system without and with phase rotation,  $M = N = 2$ .

diversity order is one, it was found that higher diversity performance is achieved in the finite SNR regime before the diversity one regime takes over, and that the diversity one regime starts at lower BER values for increased frame sizes. These observations were illustrated through a BER lower bound derived based on diversity one PEPs and simulations. Next, a phase rotation scheme using transcendental numbers was proposed to extract the full diversity offered by the delay-Doppler channel. It was proved that the proposed phase rotation achieves full diversity. Finally, we extended the diversity analysis and results for MIMO-OTFS systems without and with phase rotation.

#### REFERENCES

[1] W. C. Jakes, *Microwave Mobile Communications*, New York: IEEE Press, reprinted, 1994.  
 [2] T. Wang, J. G. Proakis, E. Masry, and J. R. Zeidler, "Performance degradation of OFDM systems due to Doppler spreading," *IEEE Trans. Wireless Commun.*, vol. 5, no. 6, pp. 1422-1432, Jun. 2006.

[3] R. Hadani, S. Rakib, M. Tsatsanis, A. Monk, A. J. Goldsmith, A. F. Molisch, and R. Calderbank, "Orthogonal time frequency space modulation," *Proc. IEEE WCNC'2017*, pp. 1-7, Mar. 2017.  
 [4] R. Hadani, S. Rakib, S. Kons, M. Tsatsanis, A. Monk, C. Ibars, J. Delfeld, Y. Hebron, A. J. Goldsmith, A. F. Molisch, and R. Calderbank, "Orthogonal time frequency space modulation," online: arXiv:arXiv:1808.00519v1 [cs.IT] 1 Aug 2018.  
 [5] R. Hadani and A. Monk, "OTFS: A new generation of modulation addressing the challenges of 5G," online: arXiv:1802.02623 [cs.IT] 7 Feb 2018.  
 [6] A. Monk, R. Hadani, M. Tsatsanis, and S. Rakib, "OTFS - orthogonal time frequency space: a novel modulation technique meeting 5G high mobility and massive MIMO challenges," online: arXiv:1608.02993 [cs.IT] 9 Aug 2016.  
 [7] R. Hadani, S. Rakib, A. F. Molisch, C. Ibars, A. Monk, M. Tsatsanis, J. Delfeld, A. Goldsmith, and R. Calderbank, "Orthogonal time frequency space (OTFS) modulation for millimeter-wave communications systems," in *Proc. IEEE MTT-S Intl. Microwave Symp.*, pp. 681-683, Jun. 2017.  
 [8] L. Li, H. Wei, Y. Huang, Y. Yao, W. Ling, G. Chen, P. Li, and Y. Cai, "A simple two-stage equalizer with simplified orthogonal time frequency space modulation over rapidly time-varying channels," online: arXiv:1709.02505v1 [cs.IT] 8 Sep 2017.  
 [9] A. Farhang, A. R. Reyhani, L. E. Doyle, and B. Farhang-Boroujeny, "Low complexity modem structure for OFDM-based orthogonal time frequency space modulation," *IEEE Wireless Commun. Lett.*, doi: 10.1109/LWC.2017.2776942, Nov. 2017.  
 [10] P. Raviteja, K. T. Phan, Q. Jin, Y. Hong, and E. Viterbo, "Low-complexity iterative detection for orthogonal time frequency space modulation," online: arXiv:1709.09402v1 [cs.IT] 27 Sep 2017.  
 [11] K. R. Murali and A. Chockalingam, "On OTFS modulation for high-Doppler fading channels," *Proc. ITA'2018*, San Diego, Feb. 2018.  
 [12] M. K. Ramachandran and A. Chockalingam, "MIMO-OTFS in high-Doppler fading channels: signal detection and channel estimation," accepted in *IEEE GLOBECOM'2018*, Dec. 2018. Online: arXiv:1805.02209v1 [cs.IT] 6 May 2018.  
 [13] A. Fish, S. Gurevich, R. Hadani, A. M. Sayeed, and O. Schwartz, "Delay-Doppler channel estimation in almost linear complexity," *IEEE Trans. Inform. Theory*, vol. 59, no. 11, pp. 7632-7644, Nov. 2013.  
 [14] D. Tse and P. Viswanath, *Fundamentals of Wireless Communication*, Cambridge University Press, 2005.  
 [15] P. J. Davis, *Circulant Matrices*, American Mathematical Society, 2012.  
 [16] M. O. Damen, A. Tewfik, and J. C. Belfiore, "A construction of a spacetime code based on number theory," *IEEE Trans. Inform. Theory*, vol. 48, no. 3, pp. 753-760, Mar. 2002.